IVYSPRING INTERNATIONAL PUBLISHER

International Journal of Medical Sciences

2026; 23(12): 3726-3743. doi: 10.7150/ijms.138218

Research Paper

Autoserum-driven Phenotypic Remodeling and Proliferative Enhancement in Human Skin-derived Mesenchymal Stromal Cells

Hui-Pu Liu[1,2,3†], Chung-Hsien Lin[2†], Chung-Chuan Hsiung[1,4], Kai-Fu Chang[2], Ching-Chung Ko[5], Hsiu-yen Sun[4], Dahlak Daniel Solomon[6,7], Sachin Kumar[6,7], Chih-Yang Wang[6,7], Ping-Lun Jiang[8], Chung-Pin Hsieh[8], Neethu Palekkode[6,7], Chung-Bao Hsieh[9,10✉], Yung-Kuo Lee[2,9,11✉], I-Hung Chen[11,12,13✉]

1. Department of General Surgery, Kaohsiung Armed Forces General Hospital, National Defense Medical University, Kaohsiung 80284, Taiwan.
2. Medical Laboratory, Medical Education and Research Center, Kaohsiung Armed Forces General Hospital, National Defense Medical University, Kaohsiung 80284, Taiwan.
3. Institute of Basic Medical Science, College of Medicine, National Cheng Kung University, Tainan 70101, Taiwan.
4. Department of Surgery, Bo-Ai Clinic, Kaohsiung, Taiwan.
5. Department of Medical Imaging, Chi-Mei Medical Center, Tainan, Taiwan.
6. PhD Program for Cancer Molecular Biology and Drug Discovery, College of Medical Science and Technology, Taipei Medical University, Taipei 11031, Taiwan.
7. Graduate Institute of Cancer Biology and Drug Discovery, College of Medical Science and Technology, Taipei Medical University, Taipei 11031, Taiwan.
8. Department of Biomedical Engineering, Medical and Pharmaceutical Industry Technology and Development Center, New Taipei City, Taiwan.
9. Division of Experimental Surgery Center, Department of Surgery, Tri-Service General Hospital, National Defense Medical Center, Taipei, Taiwan.
10. Taipei City Hospital Zhongxing Branch, Taipei City, 103212, Taiwan.
11. Institute of Medical Science and Technology, National Sun Yat-Sen University, Kaohsiung 80424, Taiwan.
12. Department of Internal Medicine, Kaohsiung Armed Forces General Hospital, National Defense Medical University, Kaohsiung 80284, Taiwan.
13. Department of Internal Medicine, Tri-Service General Hospital, National Defense Medical University, Taipei City, Taiwan.

† Equal contribution.

✉ Corresponding authors: Chung-Bao Hsieh (Email: albert0920@yahoo.com.tw), Yung-Kuo Lee (yungkuo@g-mail.nsysu.edu.tw), and I-Hung Chen (treemanhealth@gmail.com).

© The author(s). This is an open access article distributed under the terms of the Creative Commons Attribution License (https://creativecommons.org/licenses/by/4.0/). See https://ivyspring.com/terms for full terms and conditions.

Received: 2026.05.23; Accepted: 2026.09.23; Published: 2026.11.13

Abstract

Human skin dermis represents an accessible donor tissue for isolating mesenchymal stromal cells (MSCs); however, optimal *ex vivo* expansion methodologies remain to be fully established. In this study, paired skin-derived mesenchymal stromal cells (SMSCs) and adipose-derived MSCs (ADMSCs) were isolated from six adult donors undergoing benign lesion excisions. To assess donor-specific physiological expansion, SMSCs were cultured under a reduced human platelet lysate (HPL) condition (2% HPL supplemented with 10% autologous serum) through passage five and compared with isogenic 5% HPL controls. Autoserum-supplemented SMSCs adhered to International Society for Cell & Gene Therapy minimal criteria, exhibiting standard spindle morphology and characteristic surface immunophenotypes ($CD73^+$, $CD90^+$, $CD105^+$). This combined culture condition was associated with increased proliferation rates and elevated adipogenic lipid accumulation; quantitative differences between the supplemented SMSC and standard ADMSC groups were not statistically significant in this cohort, without demonstrating formal equivalence. Paired transcriptomic profiling indicated enrichment in lipid metabolic pathways, PPAR signaling, and efferocytosis, alongside significant downregulation of developmental pathways (GLI1, WNT3) and baseline lipid synthesis regulators (SCD, HMGCS1). Modest transcript-level alterations in immunomodulatory targets, including a nominal increase in PECAM1, were also observed. Adult skin dermis yields stromal populations meeting standard MSC phenotypic benchmarks. While this reduced-HPL/autoserum regimen modulates transcriptomic profiles and enhances adipogenic differentiation, gene expression shifts alone do not establish functional immunosuppressive capacity, necessitating direct functional immunological evaluation in future investigations.

Keywords: mesenchymal stromal cells; skin-derived MSCs; autologous serum; *ex vivo* priming; trilineage differentiation; RNA sequencing; reduced HPL; donor variability

Introduction

Mesenchymal stromal cells (MSCs) have become one of the most widely investigated cell populations in regenerative medicine, with clinical applications spanning inflammatory diseases, tissue repair, graft versus host disease, and immune modulation [1, 2]. As articulated in updated ISCT guidance on MSC nomenclature and mechanism of action [3], their therapeutic utility is primarily attributed to a paracrine secretome rather than direct engraftment and transdifferentiation. This secretome, comprising anti-inflammatory cytokines, trophic growth factors, and extracellular vesicles (EVs), functions to activate resident tissue progenitor cells and suppress pathological immune responses [4, 5]. MSCs are now fundamentally redefined as multipotent stromal cells *in vitro* that orchestrate tissue homeostasis and immune regulation upon *in vivo* deployment. The choice of tissue source substantially influences the biological properties of the resultant MSC population. Adipose tissue has largely superseded bone marrow as the preferred source for clinical production owing to its high MSC density [6]. However, adipose tissue harvest requires dedicated surgical intervention, and donor site availability may be limited in pediatric, cachectic, or medically complex patients. Skin represents a promising yet underexplored alternative. As the largest organ of the human body, skin harbors cellular constituents derived from two embryonic germ layers, ectoderm (keratinocytes, melanocytes) and mesoderm (dermal fibroblasts, vascular cells), together with a neural crest-derived population that migrates from the dorsal neural tube during development [7]. Neural crest is an ectodermal derivative rather than a distinct primary germ layer. The embryological heterogeneity of the dermal niche represents a biologically plausible, though not yet experimentally demonstrated, basis for exploring skin as an MSC source.

While full-thickness skin biopsies offer a minimally invasive procurement route that, in principle, is not restricted by donor sex, in contrast to foreskin-derived sources, current SMSC research has predominantly relied on foreskin tissue. This reliance presents a translational bottleneck: foreskin is strictly sex-limited and primarily harvested from pediatric populations, precluding its use as an autologous source for adult females or the broader patient demographic. Establishing a protocol utilizing adult, non-foreskin skin biopsies is therefore essential for equitable clinical translation.

Equally critical to cell sourcing is the *ex vivo* expansion microenvironment. Standard paradigms increasingly utilize HPL to avoid the immunogenic and regulatory risks of fetal bovine serum (FBS) [8-10]. While HPL supports proliferation, it provides an idealized, stress-free microenvironment devoid of the pathological or inflammatory signals the cells will encounter upon clinical infusion. Autologous serum derived from the patient's own peripheral blood offers a conceptually distinct advantage. Because autologous serum directly reflects the patient's individual inflammatory milieu, circulating cytokine profile, growth factor concentrations, and disease-specific molecular signals, it may serve as a personalized physiological primer for MSC expansion [11-15]. This rationale has been formalized as Disease Microenvironment Preconditioning (DMP): exposure of MSCs to patient-derived serum or body fluids may strengthen their adaptation to the post-infusion environment [11, 12].

We hypothesize that supplementing culture media with autologous serum may prime the MSCs prior to reinfusion, transcriptionally tuning their secretory program to the donor's pathological context. Priming approaches have been shown to transcriptionally and functionally reprogram the MSC secretome, via RAB27B-dependent biogenesis pathways [13, 14]. This pre-conditioning strategy is analogous to immunological priming: just as adaptive immune cells acquire antigen-specific memory through prior exposure, autoserum-cultured MSCs may acquire disease-specific paracrine competence, preparing them to respond to complex inflammatory or fibrotic microenvironments [16, 17].

To date, the combined effects of an accessible adult skin source and an autologous serum priming strategy on SMSC identity, proliferative performance, and transcriptomic programming have not been systematically evaluated in a single isogenic study. In the present work, we systematically characterized SMSCs expanded under a physiological priming paradigm utilizing reduced HPL (2%) supplemented with autologous serum, benchmarked against standard 5% HPL-expanded SMSCs and isogenic ADMSCs. We aimed to characterize how this combined priming paradigm modulates multipotency, particularly the PPARγ-driven adipogenic axis, which is increasingly recognized as a metabolic factor associated with MSC immunomodulatory function, and to describe the transcriptomic landscape associated with this culture strategy as a hypothesis-generating basis for future functional validation.

Materials and Methods

Donor selection and tissue procurement

Following clinical screening and the procurement

of written informed consent, paired samples of full-thickness skin and subcutaneous adipose tissue were obtained from six independent human donors (n = 6) undergoing surgical excision for epidermal cyst or lipoma. To minimize donor site morbidity while securing sufficient progenitor populations, the skin biopsy was standardized to a minimal periumbilical excision of approximately 0.5 cm². Peripheral blood (120-150 mL) was collected simultaneously into serum-separator tubes without anticoagulant and allowed to clot at room temperature for 30 minutes prior to centrifugation for patient-specific serum preparation [18-20]. The study was conducted in accordance with the Declaration of Helsinki and approved by the Institutional Review Board of the Armed Forces Kaohsiung General Hospital (IRB approval no. KAFGHIRB-114-001). Donor demographic and clinical characteristics, including age, sex, and clinical indication, are summarized in Table 1. The autologous serum used for each donor's preconditioning was derived from the same individual's peripheral blood, ensuring that the serum composition was donor-specific and reflective of each patient's circulating cytokine and growth factor profile.

Table 1. Donor demographics

Donor ID	Age	Sex	Clinical Indication	Serum Type	Tissue Source
D1	31	Male	Epidermal cyst	Autologous	Skin + Adipose
D2	44	Male	Lipoma	Autologous	Skin + Adipose
D3	36	Male	Epidermal cyst	Autologous	Skin + Adipose
D4	58	Female	Lipoma	Autologous	Skin + Adipose
D5	60	Male	Epidermal cyst	Autologous	Skin + Adipose
D6	62	Female	Lipoma	Autologous	Skin + Adipose

Isolation of skin-derived and adipose-derived MSCs

Skin-derived mesenchymal stromal cells and matched adipose-derived mesenchymal stromal cells were isolated from full-thickness skin and subcutaneous adipose tissue, respectively, and provided as passage 0 (P0) by Kaohsiung Bo-Ai Clinic, where tissue decontamination, enzymatic digestion, and initial seeding were performed according to the facility's established tissue-processing protocols. Upon receipt, P0 SMSCs were expanded in α-MEM basal medium supplemented with 5% HPL, whereas ADMSCs were expanded in α-MEM supplemented with 5% HPL. Upon reaching 70-80% confluency, cells were enzymatically detached using TrypLE Select (Gibco) and re-seeded into T-175 flasks at a density of 4,000-5,000 cells/cm².

Autologous serum preparation and biphasic culture paradigm

To derive the autologous serum supplement, the collected whole blood in serum-separator tubes was allowed to clot at room temperature for 30 minutes, then subjected to centrifugation at 3,000 × g for 15 minutes to separate the serum fraction. The serum was processed through two freeze-thaw cycles (−80°C to room temperature) to release platelet-derived growth factors. The processed product was then subjected to a second centrifugation at 3,000 × g for 15 minutes to remove cellular debris. The final serum fraction was sterile filtered through a 0.22 μm membrane and stored at −80°C until use. To achieve sufficient cellular yield while imparting physiological preconditioning, a biphasic culture strategy was employed for the SMSCs. During the initial bulk expansion phase (Passages 1-2), isolated SMSCs were cultured in α-MEM basal medium supplemented with 5% HPL to support proliferation. Beginning at Passage 3, we transitioned the culture microenvironment to the priming phase by supplementing the basal medium (α-MEM) with 2% HPL and 10% (v/v) autologous serum, maintained from Passage 3 through Passage 5. Proliferation kinetics (PDT and PDL) were tracked from P2 through P5, with the priming effect reflected in the P3-P5 interval.

Cell proliferation kinetics

Cellular proliferation and expansion dynamics were monitored from Passage 2 (P2) through Passage 5 (P5). Viable cell counts and viability percentages were determined using a Countess II Automated Cell Counter (Thermo Fisher Scientific). The Population Doubling Level (PDL) for each passage was calculated using the formula: $PDL = 3.322 \times (\log Cf - \log Ci)$, where Cf represents the final harvest cell number, and Ci represents the initial seeding cell number. The doubling time (DT) in hours was determined using the formula: $DT = [T \times \ln(2)] / \ln(Cf / Ci)$, where T represents the total culture duration in hours. Because PDT and PDL were measured repeatedly within the same donor-derived cultures across passages, proliferation kinetics were analyzed using a linear mixed-effects model with donor as a random effect and condition × passage as fixed effects, focusing on the Passage 3-5 interval during which autoserum supplementation was active. Six biological replicates (n = 6 donors) were used per group.

Flow cytometry and immunophenotypic characterization

To confirm MSC identity according to the ISCT minimal criteria, surface marker expression was analyzed at Passage 2 and Passage 5. Cells were gently

detached using Accutase and incubated with fluorochrome-conjugated monoclonal antibodies against CD90-FITC (BD Biosciences, Cat #51-9007657), CD105-PerCP-Cy5.5 (BD Biosciences, Cat #51-9007648), and CD73-APC (BD Biosciences, Cat #51-9007649), together with the hMSC Positive Isotype Control Cocktail (BD Biosciences, Cat #51-9007664). The negative exclusion cocktail comprised PE-conjugated antibodies against CD34, CD45, CD11b, CD19, and HLA-DR (BD Biosciences, Cat #51-9007661; isotype control Cat #51-9007662), supplemented with CD14-BV785 (BioLegend, Cat #367141; isotype control Cat #400169). Viable cells were identified by DAPI exclusion. Flow cytometric acquisition was performed on a CytoFLEX LX flow cytometer (Beckman Coulter), and data were analyzed using CytExpert software to ensure cells met ISCT minimal criteria (≥95% positive markers; ≤2% negative markers) [21-23]. The gating hierarchy for flow cytometric analysis was as follows: (1) a forward scatter (FSC) vs. side scatter (SSC) gate was applied to identify the nucleated cell population and exclude debris; (2) a forward scatter height (FSC-H) vs. forward scatter area (FSC-A) gate was used to exclude doublets and aggregates, retaining singlet events; (3) viable cells were identified by negative DAPI staining for live/dead discrimination; (4) marker expression analysis was performed exclusively on the live singlet population. Positive markers (CD73, CD90, CD105) were evaluated against fluorescence-minus-one (FMO) controls, and negative markers (CD14, CD45, CD34, CD11b, CD19, HLA-DR) were assessed using the same gated population.

In vitro trilineage differentiation assays

All trilineage differentiation assays were performed on cells at Passage 5, matching the passage at which RNA sequencing and flow cytometry were conducted. The multilineage developmental plasticity of isolated cells was evaluated using standardized directed differentiation protocols. For adipogenesis, cells were cultured in StemPro Adipogenesis Differentiation Kit medium (Gibco) according to the manufacturer's instructions without modification; intracellular lipid accumulation was visualized by Oil Red O (ORO) staining on Day 9 and Day 21 for both ADMSC and SMSC (matched time points for both cell types). For osteogenesis, cells were cultured in StemPro Osteogenesis Differentiation Kit medium (Gibco) without modification for 21 days; extracellular matrix mineralization was assessed by Alizarin Red S (ARS) staining. Chondrogenic differentiation was performed in a 3D pellet culture system: cells (2.5×10^5 per pellet) were centrifuged in 15 mL conical tubes to form high-density micromasses and cultured in StemPro Chondrogenesis Differentiation Kit medium (Gibco) without modification for 20 days. Chondrogenesis was evaluated by macroscopic pellet diameter measurement and confirmed by Alcian Blue staining for glycosaminoglycan synthesis. Non-induced control cultures were maintained in parallel for all conditions. For quantitative analysis of lineage-specific staining, microscopic images were analyzed using ImageJ software (National Institutes of Health, Bethesda, MD, USA). Images were acquired under identical imaging conditions for the corresponding control and differentiation groups. Staining-positive regions were identified using a consistent thresholding method, and the percentage of positive staining area was calculated as the positively stained area divided by the total analyzed area × 100%. Oil Red O- and Alizarin Red S-positive areas were quantified as indicators of adipogenic and osteogenic differentiation, respectively. Multiple representative fields were analyzed for each sample, and the mean percentage of positive staining area was used for statistical analysis.

RNA sequencing and transcriptomic analysis

Total RNA was extracted from passage 5 cells (n = 6 donors per group; 18 samples total) using the RNeasy Mini Kit (Qiagen). Samples with RNA Integrity Number ≥8 were processed for library preparation using the TruSeq Stranded mRNA Library Prep Kit (Illumina). Paired-end sequencing (150 bp) was performed on the Illumina NovaSeq 6000 platform at ≥20 million reads per sample. Reads were aligned to the GRCh38 human reference genome using STAR v2.7, and gene-level expression was quantified using RSEM v1.3. Differentially expressed genes (DEGs) were identified from RSEM-derived expected counts using DESeq2 with a paired design (~donor + condition), with Benjamini-Hochberg adjusted p value < 0.05 and $|\log_2 FC| > 1$ as cutoffs [24-30]. Transcripts per million (TPM) values were used for visualization and targeted gene panel analyses only. KEGG pathway enrichment analysis was performed using clusterProfiler v4.0 in R v4.4.3. PCA and Pearson correlation heatmap analysis were performed on $\log_2$-transformed TPM matrices. Targeted gene expression was visualized as boxplots and dumbbell plots with expression values reported as $\log_2$ (TPM + 1).

Statistical analysis

Unless otherwise specified, data are presented as mean ± standard deviation (SD). For proliferation kinetics, a linear mixed-effects model was used with donor as a random effect and condition × passage as fixed effects, focusing on the Passage 3-5 interval. For differentiation assays, two-group comparisons were performed using a two-tailed Student's t-test. For

RNA-seq data, all transcriptomic comparisons employed a paired analysis framework that accounts for the isogenic donor design [30-34]. Targeted gene panel comparisons (SMSC HPL vs. SMSC Auto) were performed using the Wilcoxon signed-rank test on $\log_2(TPM + 1)$ values, paired by donor, with Benjamini-Hochberg false discovery rate (FDR) correction applied across all genes tested within each functional panel (FDR-adjusted $p < 0.05$). For each gene, the paired mean difference (effect size) and 95% confidence interval were reported. We note that with $n = 6$ paired donors, the exact Wilcoxon signed-rank test has limited resolution near $p = 0.05$, and results should be interpreted accordingly. Global differentially expressed gene (DEG) analysis was performed using DESeq2 on RSEM-derived expected counts with a paired design (~ donor + condition), incorporating donor as a factor to account for inter-donor variability, with an adjusted p value < 0.05 and $|\log_2FC| > 1$ as cutoffs [34-37]. Statistical analyses were conducted in Prism 9.0 and R v4.4.3. Significance thresholds: *FDR-adjusted $p < 0.05$; **FDR-adjusted $p < 0.01$; ns, not significant.

Results

1. Isolation, morphological characterization, and physiological priming of human skin-derived cells under the combined paradigm

To rigorously evaluate adult skin as a clinically accessible source and address translational hurdles, we successfully isolated human skin-derived cells alongside matched adipose-derived counterparts from six independent donors. Under standard expansion conditions, both cell populations exhibited canonical fibroblast-like, spindle-shaped morphology at passage 5 (Figure 1A). Transitioning skin-derived cells to the physiological priming paradigm utilizing autologous serum did not elicit adverse morphological alterations (Figure 1A). In three of the six donors (Donors 1–3), SMSCs cultured under the autoserum-supplemented condition displayed an interconnected network-like morphology distinct from the standard spindle shape observed in the other conditions; the functional implications of this phenotypic variant warrant further investigation and represent a study limitation. Proliferation kinetics revealed a marked functional divergence: despite the substantial reduction of human platelet lysate from 5% to 2%, the concomitant supplementation with 10% autologous serum supported robust expansion, significantly accelerating proliferation rates, shortening doubling times, and yielding higher cumulative population doublings relative to standard controls within this cohort (Figures 1B and 1C).

2. Immunophenotypic characterization confirms compliant identity across culture paradigms

Surface marker expression profiles were evaluated by multi-parameter flow cytometry to confirm cell identity against established criteria. Across all six paired donors, both adipose-derived and skin-derived cells consistently expressed the canonical markers CD73, CD90, and CD105 (Figure 2A). These populations remained strictly negative for the hematopoietic exclusion markers assessed (CD14, CD45, CD34, CD11b, CD19, HLA-DR) (Figure 2B). We note that CD14 and CD45 are hematopoietic rather than endothelial markers, and that our exclusion panel did not include CD31 (PECAM1) itself. Given the significant upregulation of PECAM1 observed by RNA-seq, validating CD31 protein expression by flow cytometry is identified as a priority for future work to determine whether this reflects a discrete $CD31^+$ subpopulation rather than a uniform shift across the SMSC population. The results demonstrate that the proliferative enhancements observed in the autoserum group were achieved without compromising the fundamental immunophenotype of the cells.

3. The autoserum-containing priming paradigm is associated with enhanced adipogenic potential and preserved trilineage competence

To evaluate developmental plasticity, the isogenic cohorts were subjected to standardized differentiation protocols. Under standard conditions, skin-derived cells successfully differentiated into osteoblasts and chondrocytes, confirming trilineage competence; however, quantitative mineralization was significantly lower in SMSCs than in ADMSCs (Figure 4B), while chondrogenic pellet expansion did not differ significantly between cell types (Figure 5B). Standard skin-derived cells exhibited a notably constrained adipogenic potential relative to adipose-derived cells (Figure 3). Preconditioning with autologous serum increased lipid vacuole formation in skin-derived cells; the difference between SMSC + autoserum and ADMSC + 5% HPL groups was not statistically significant in this cohort (Figure 3B), though this should not be interpreted as formal equivalence, which would require a predefined equivalence margin and non-inferiority analysis not performed here. Autoserum supplementation did not significantly alter either osteogenic or chondrogenic output relative to SMSC + 5% HPL controls (Figures 4 and 5).

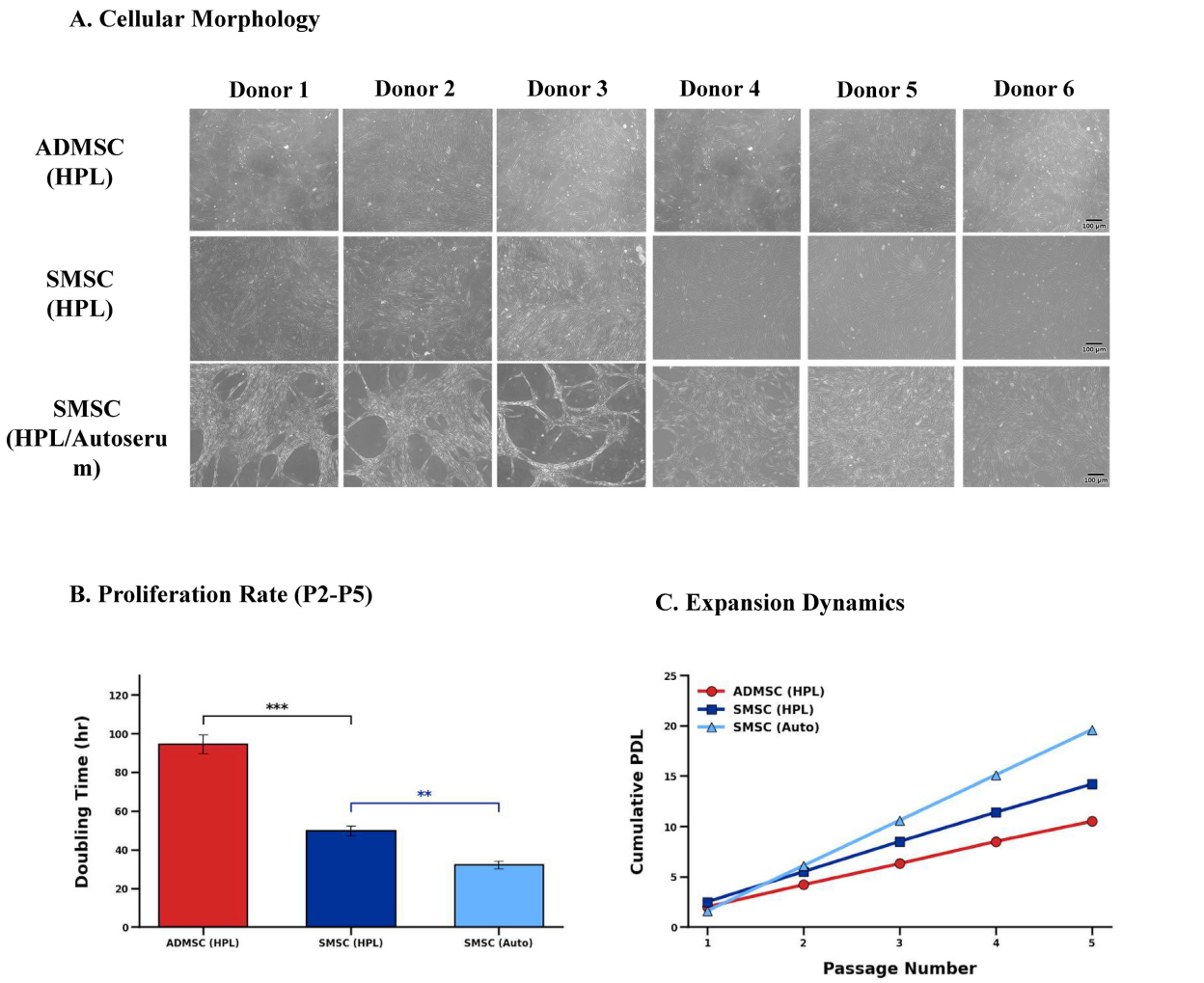


Figure 1. Morphology and proliferation kinetics of SMSCs under standard and priming conditions. (A) Representative phase contrast microscopic images of ADMSC (5% HPL), SMSC (5% HPL), and SMSC (2% HPL + Autoserum) from six paired donors at passage 5. Scale bar: 100 µm. (B) Population doubling time (PDT, hours) across passages 2-5, presented as an XY plot to visualize the divergence emerging at Passage 3, when autoserum supplementation began. (C) Cumulative population doubling level (PDL) over passages 2-5. Data: mean ± SD (n = 6 paired donors). **p < 0.01; ***p < 0.001.

4. Global transcriptomic profiling reveals donor-consistent reprogramming

Global RNA sequencing demonstrated that autologous serum preconditioning is associated with broad transcriptomic shifts rather than superficial fluctuations. Principal component analysis and correlation analysis showed distinct clustering driven by both cell origin and serum conditions (Figure 6A). Using a paired design that accounted for the isogenic donor structure, analysis of differentially expressed genes between the primed and standard groups revealed enrichment in PPAR signaling, fat digestion, and efferocytosis pathways (Figure 6C). Because pathway enrichment reflects over-representation of DEGs rather than net pathway activity, we do not interpret these results as evidence of pathway "activation"; the directionality of individual constituent genes is reported separately in Figures 7 and 8. These findings indicate that autoserum preconditioning is associated with consistent transcriptomic shifts across the independent donors, with the most prominent changes concentrated in lipid metabolism and developmental signaling pathways.

5. Targeted interrogation of RNA-seq signatures reveals discrete shifts in developmental and metabolic gene panels

Targeted gene panel analysis was performed by comparing SMSC cultured in 5% HPL versus SMSC cultured in 2% HPL + autoserum, using $\log_2$-transformed transcripts per million values across the six paired donors, with paired Wilcoxon signed-rank tests and Benjamini-Hochberg false discovery rate (FDR) correction applied within each panel (Figure 7 and Figure 8; Table 2). The most consistent transcriptomic changes, surviving FDR correction, were concentrated in two domains. First, in the lipid and PPAR metabolism panel, a statistically significant decrease was observed in three key regulators (SCD, Δ

= −1.69, 95% CI [−2.47, −0.91]; HMGCS1, Δ = −1.65, [−2.05, −1.26]; and SORBS1, Δ = −0.37, [−0.55, −0.19]), all with p = 0.036 and FDR = 0.036 (Figures 7D and 8J). Second, components of the Hedgehog and Wnt pathways, specifically GLI1 (Δ = −1.17, [−1.67, −0.67]), GLI2 (Δ = −1.39, [−1.98, −0.79]), and WNT3 (Δ = −0.72, [−1.15, −0.30]), were significantly downregulated in the primed cells (all p = 0.036, FDR = 0.036; Figures 7D and 8H).

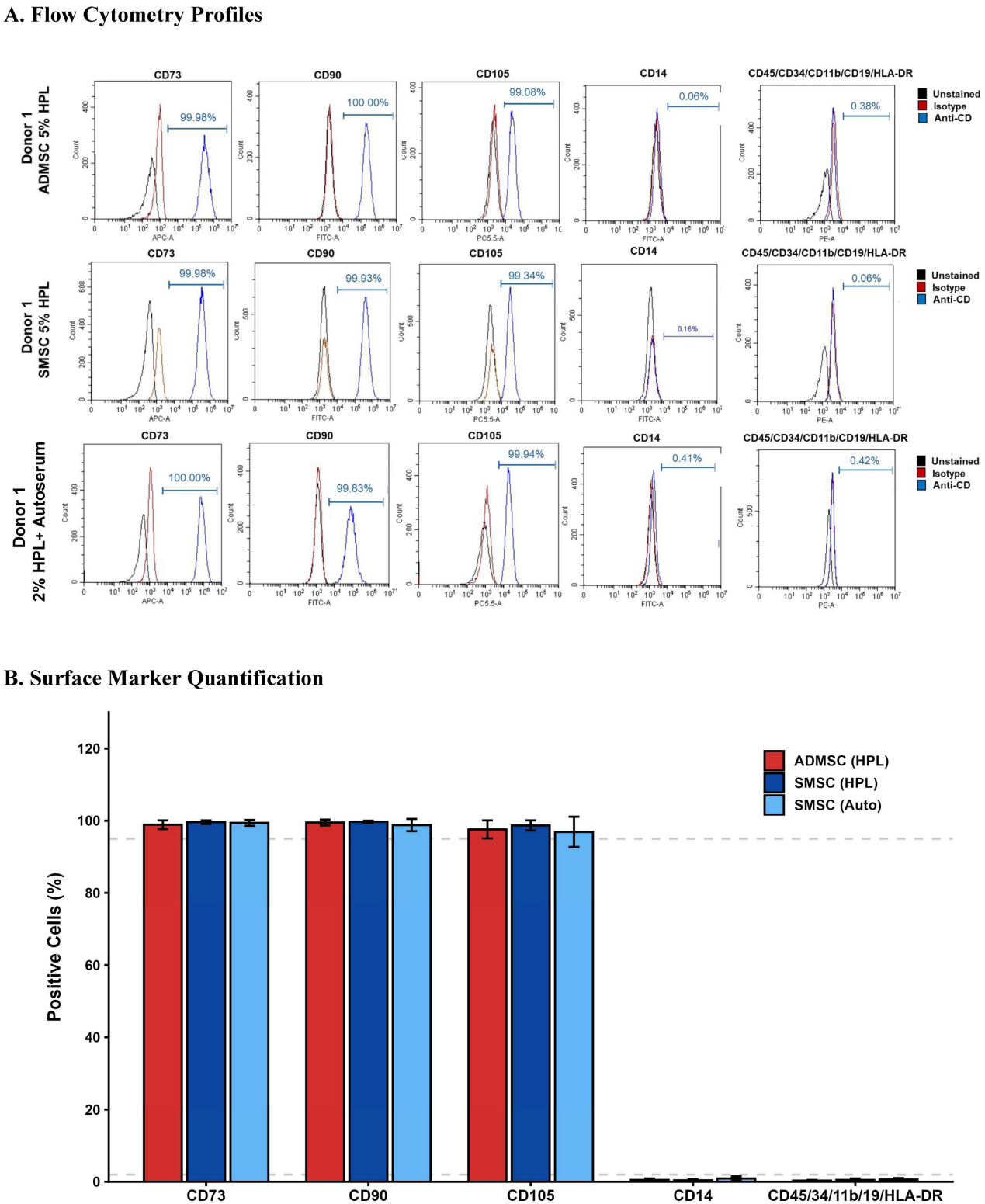


Figure 2. ISCT-compliant immunophenotypic characterization of expanded MSCs. (A) Representative flow cytometry histograms for positive markers (CD73, CD90, CD105) and negative marker cocktail (CD14, CD45, CD34, CD11b, CD19, HLA-DR) across all three groups at passage 5. Dashed grey lines indicate ISCT thresholds (≥95% positive; ≤2% negative). (B) Quantitative bar graphs aggregated across six paired donors. Data: mean ± SD (n = 6).

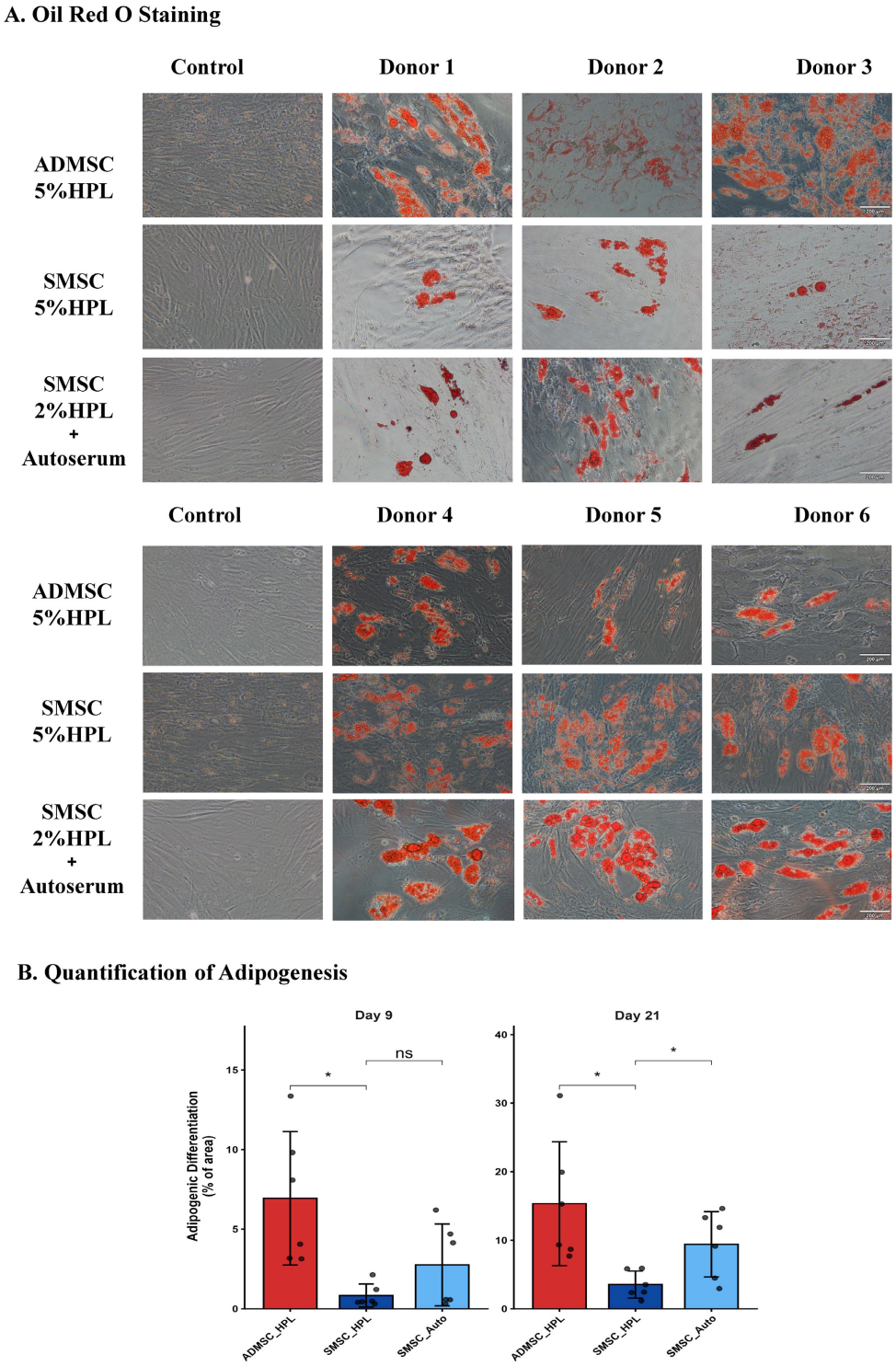


Figure 3. Adipogenic differentiation potential. (A) Oil Red O staining images at Day 21 post-induction across six paired donors. Non-induced controls shown on left. Scale bar: 200 µm. (B) Quantification of ORO-stained lipid area at Days 9 and 21 for both ADMSC and SMSC (matched time points). Data: mean ± SD (n = 6). Student's t-test (paired by donor). *p < 0.05; ns, not significant.

Beyond these FDR-significant changes, several genes showed nominally significant alterations ($p < 0.05$) with consistent directional changes across all six donors that did not survive FDR correction. Within the stemness panel, SOX2 showed nominally significant upregulation in the SMSC + autoserum group relative to SMSC + 5% HPL controls ($p = 0.036$, FDR = 0.089) and KLF4 exhibited a consistent upward trend ($p = 0.059$, FDR = 0.089) across the six paired donors (Figures 7A and 8B). In the efferocytosis panel, PECAM1 showed nominal statistical significance (upregulated; $p = 0.036$, FDR = 0.079), while DUSP4 (p

= 0.059, FDR = 0.079) and PTGER2 (p = 0.059, FDR = 0.079) showed consistent upward trends (Figures 7D and 8I). Adipogenic markers PPARG (p = 0.036, FDR = 0.054) and FABP4 (p = 0.036, FDR = 0.054) were also nominally significant. The mitogenic receptor PDGFRB exhibited a decrease in the autoserum-primed group but did not reach statistical significance (p = 0.142, FDR = 0.213) (Figures 7B and 8G), a finding we discuss further in the revised Discussion. Together, these observations suggest a reproducible biological response to the combined priming paradigm, with consistent transcriptomic changes in lipid metabolism and developmental signaling pathways, complemented by consistent but less statistically stringent trends in stemness, immunomodulatory, and adipogenic marker expression.

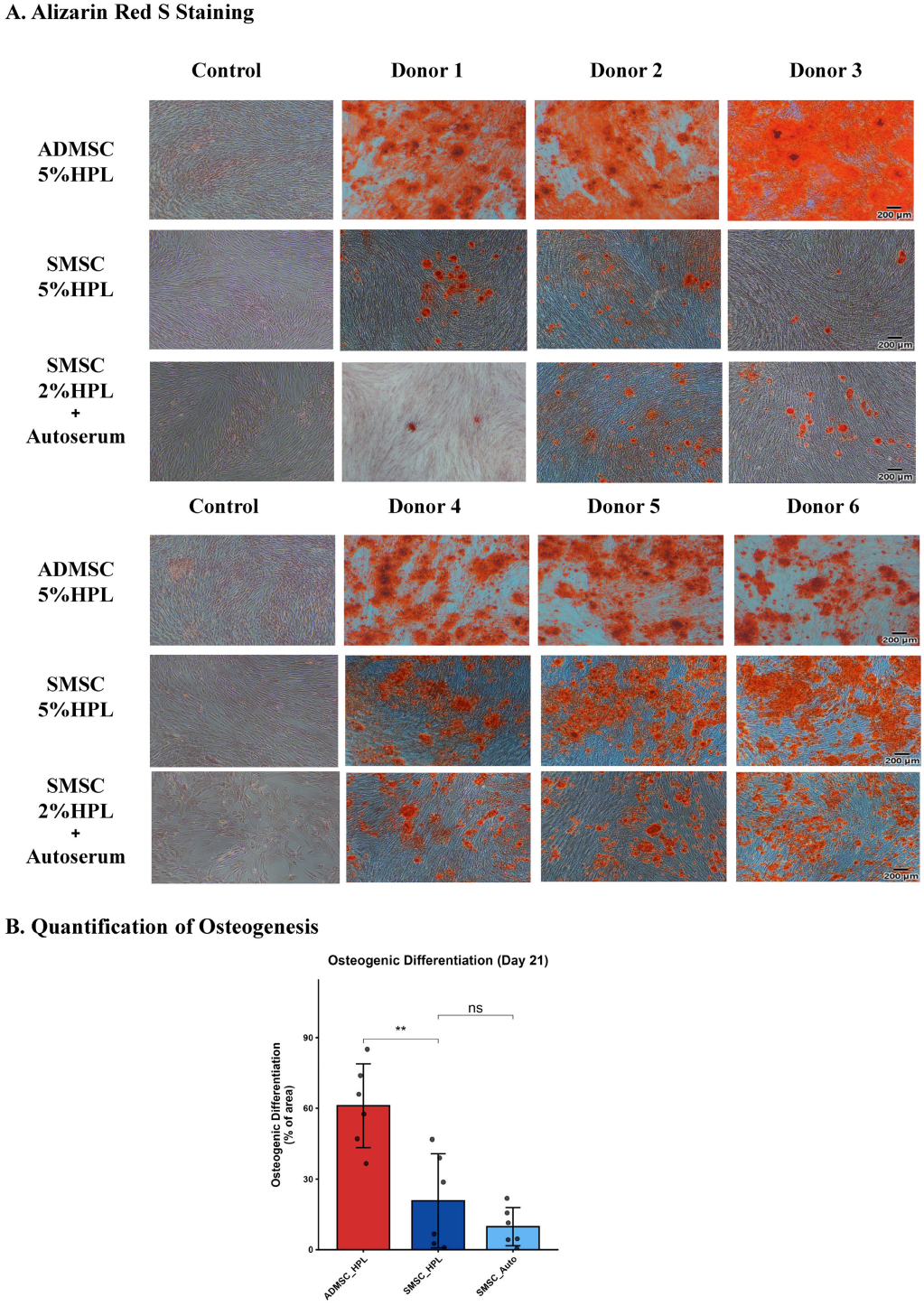


Figure 4. Osteogenic differentiation potential. (A) Alizarin Red S staining at Day 21 post-induction across six paired donors. Non-induced controls shown on left. Scale bar: 200 µm. (B) Percentage mineralized area. Data: mean ± SD (n = 6). Student's t-test (paired by donor). **p < 0.01; ns, not significant.

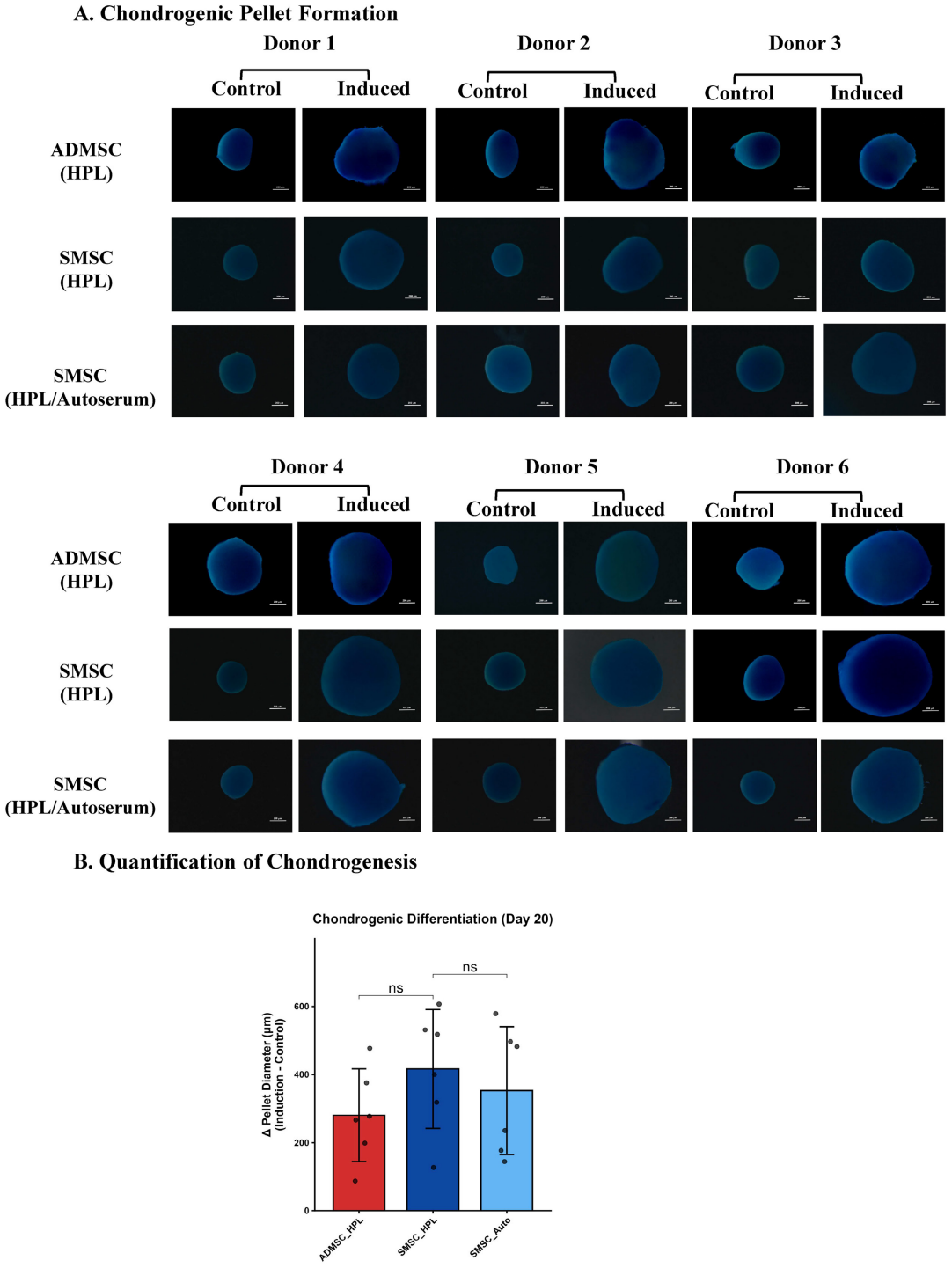


Figure 5. Chondrogenic differentiation potential. (A) Macroscopic images of 3D pellets at Day 20 (Control vs. Induced) across six paired donors. (B) Net increase in pellet diameter (ΔDiameter = Induced - Control) and representative Alcian Blue staining confirming glycosaminoglycan synthesis. Data: mean ± SD (n = 6). Student's t-test (paired by donor). ns, not significant.

Discussion

The present study establishes human adult skin dermis as a minimally invasive and readily accessible mesenchymal stromal cell source that meets ISCT immunophenotypic and trilineage differentiation criteria; functional therapeutic potency was not assessed in this study. Our findings collectively indicate that a reduced-HPL/autoserum priming paradigm, combining 2% HPL and 10% autologous serum, is associated with enhanced expansion and consistent transcriptomic shifts in skin-derived cells within the study cohort. By utilizing an isogenic donor design, we minimized genetic confounding factors to examine how the combined priming microenvironment modulates the biological identity

of these cells. We note that the priming condition differs from the standard 5% HPL control in two simultaneous variables (HPL concentration, autoserum supplementation), which precludes attributing the observed effects to any single component; this is discussed explicitly as a limitation (see the Study limitations and future directions section below).

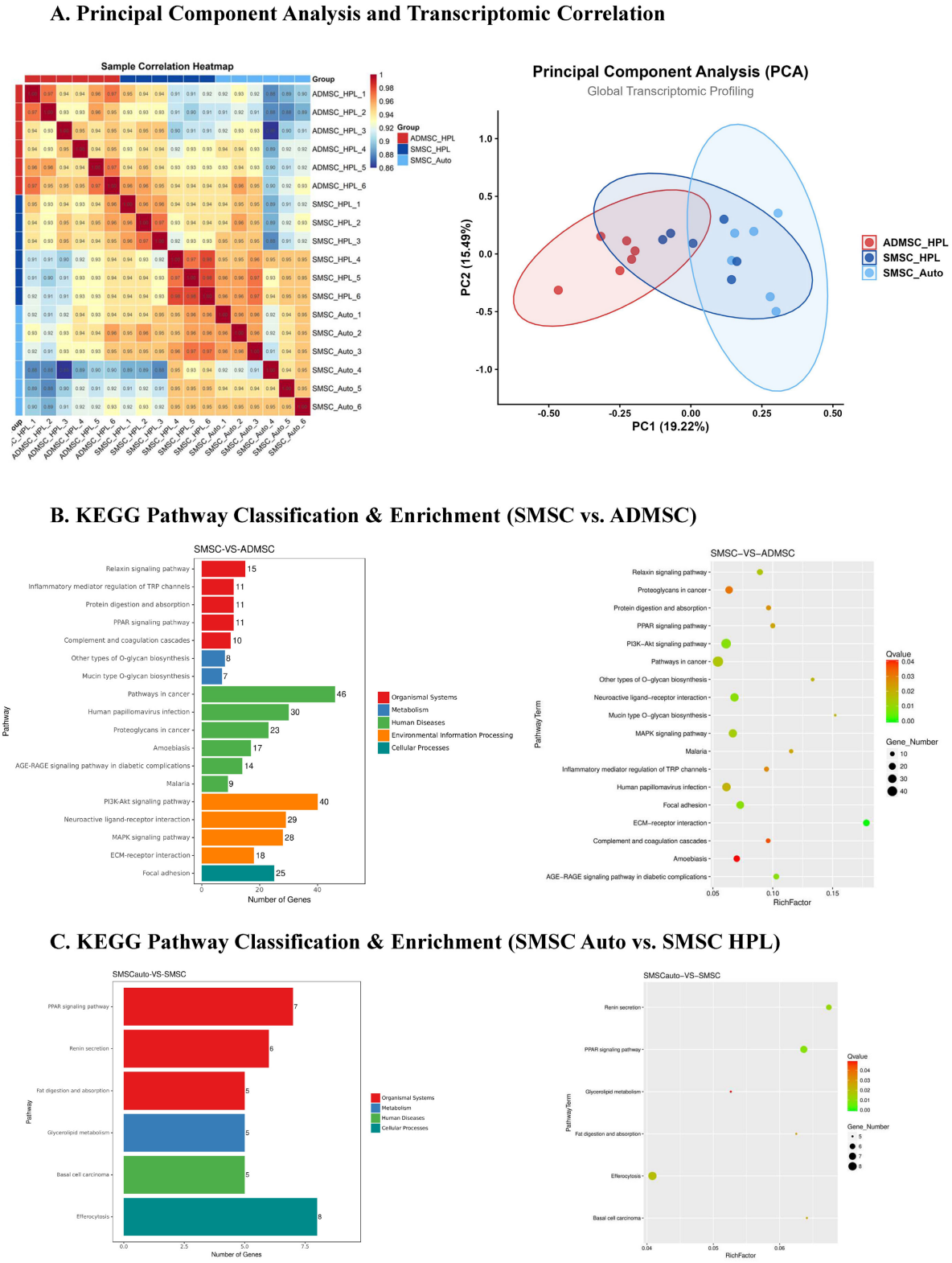


Figure 6. Global transcriptomic profiling and KEGG pathway enrichment analysis. (A) PCA plot and Pearson correlation heatmap of 18 RNA-seq samples (ADMSC HPL, SMSC HPL, SMSC Auto; n = 6 per group). (B) KEGG functional classification bar chart for DEGs between SMSC and ADMSC. (C) KEGG bubble plot for DEGs between SMSC Auto and SMSC HPL, highlighting PPAR signaling, glycerolipid metabolism, and efferocytosis as top priming-responsive pathways. X axis in bubble plot: RichFactor; bubble size: DEG count; color: Q value.

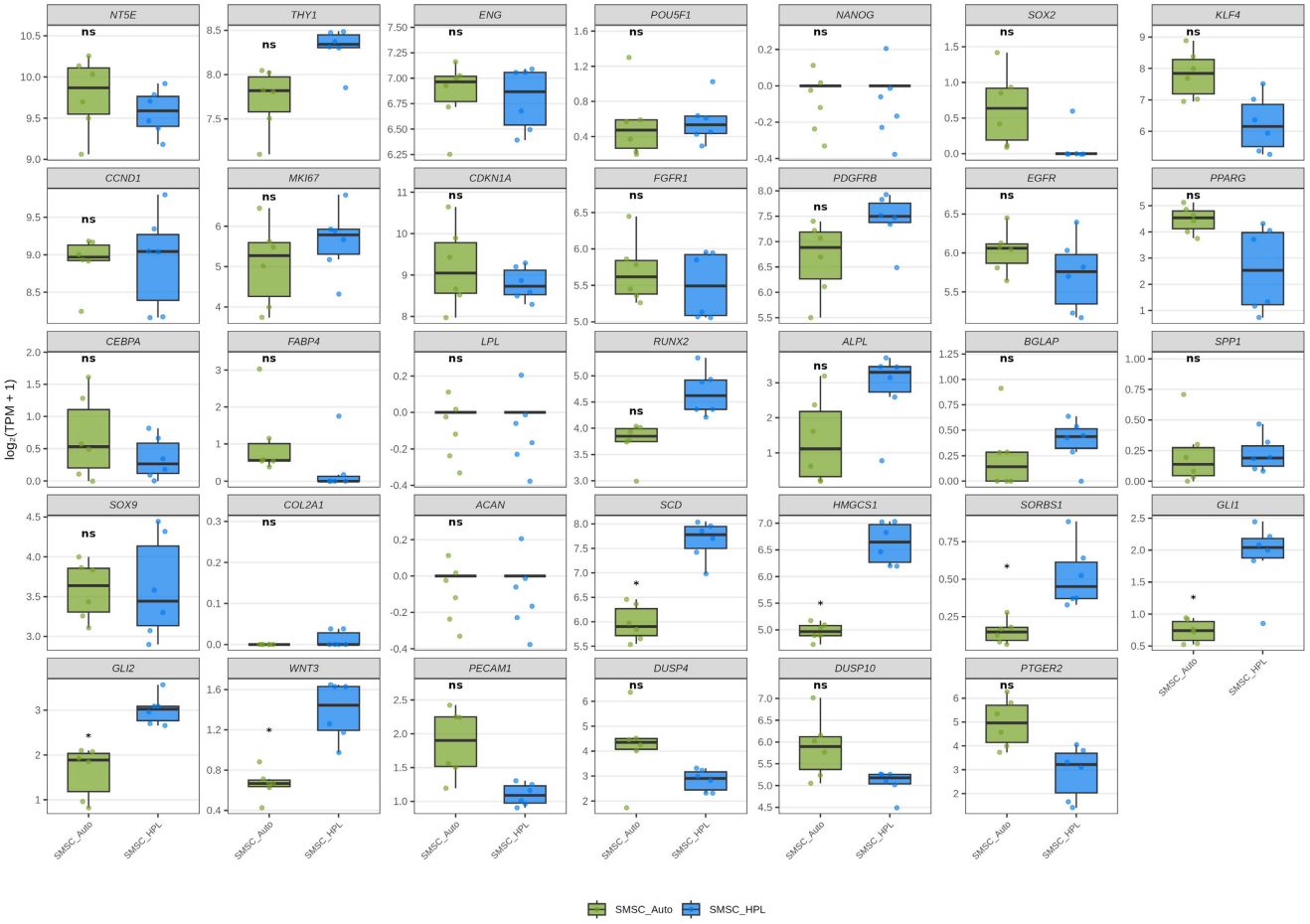


Figure 7. Targeted transcriptomic profiling of MSC signatures and KEGG enriched regulators. Boxplots [$\log_2$(TPM + 1)] comparing SMSC HPL vs. SMSC Auto for: (A) immunophenotypic markers (NT5E, THY1, ENG) and stemness (POU5F1, NANOG, SOX2, KLF4); (B) cell cycle (CCND1, MKI67, CDKN1A) and mitogenic receptors (FGFR1, PDGFRB, EGFR); (C) adipogenic (PPARG, CEBPA, FABP4, LPL), osteogenic (RUNX2, ALPL, BGLAP, SPP1), chondrogenic (SOX9, COL2A1, ACAN) markers; (D) KEGG enriched signatures: lipid/PPAR (SCD, HMGCS1), Hedgehog/Wnt (GLI1, WNT3), efferocytosis (DUSP4). Individual dots: n = 6. Paired Wilcoxon signed-rank test with Benjamini-Hochberg FDR correction. *FDR-adjusted $p < 0.05$; **FDR-adjusted $p < 0.01$; ns, not significant. Effect sizes (paired mean difference) and 95% confidence intervals are reported in Table 2.

Table 2. A comprehensive table containing all statistical results

Panel	Gene	Ref mean	Treat mean	Mean diff	Ci lower	Ci upper	Wilcox p-value	Wilcox P-adj	t_p	t_padj	Rank biserial
Immunophenotypic	NT5E	9.5738	9.7808	0.2070	-0.4711	0.8851	0.6750	0.8339	0.4682	0.7023	0.2381
Immunophenotypic	THY1	8.3005	7.7180	-0.5825	-1.1024	-0.0626	0.0592	0.1775	0.0346	0.1038	-0.9048
Immunophenotypic	ENG	6.7946	6.8474	0.0528	-0.4124	0.5180	0.8339	0.8339	0.7822	0.7822	0.1429
Stemness	POU5F1	0.5758	0.5451	-0.0307	-0.3003	0.2389	1.0000	1.0000	0.7816	0.7816	-0.0476
Stemness	NANOG	0.0000	0.0000	0.0000	0.0000	0.0000	NA	NA	NA	NA	NA
Stemness	SOX2	0.0988	0.6398	0.5410	-0.0143	1.0962	0.0360	0.0888	0.0542	0.0813	1.0000
Stemness	KLF4	6.2467	7.8214	1.5747	0.1213	3.0281	0.0592	0.0888	0.0387	0.0813	0.9048
Cell cycle	CCND1	8.9290	8.9090	-0.0200	-1.0310	0.9910	0.8339	0.8339	0.9614	0.9614	-0.1429
Cell cycle	MKI67	5.6338	5.0592	-0.5746	-2.3367	1.1875	0.2945	0.6025	0.4401	0.6777	-0.5238
Cell cycle	CDKN1A	8.7917	9.1895	0.3978	-0.8560	1.6516	0.4017	0.6025	0.4518	0.6777	0.4286
Mitogenic	FGFR1	5.5029	5.6944	0.1916	-0.0512	0.4343	0.1422	0.2133	0.0983	0.1616	0.7143
Mitogenic	PDGFRB	7.4315	6.6691	-0.7624	-1.7640	0.2392	0.1422	0.2133	0.1078	0.1616	-0.7143
Mitogenic	EGFR	5.7243	6.0257	0.3013	-0.3870	0.9897	0.2945	0.2945	0.3115	0.3115	0.5238
Adipogenic	PPARG	2.5587	4.4700	1.9113	0.6353	3.1873	0.0360	0.0540	0.0120	0.0180	1.0000
Adipogenic	CEBPA	0.3512	0.6772	0.3260	-0.3986	1.0506	0.2945	0.2945	0.2997	0.2997	0.5238
Adipogenic	FABP4	0.3218	1.0396	0.7178	0.3043	1.1312	0.0360	0.0540	0.0066	0.0180	1.0000
Adipogenic	LPL	0.0000	0.0000	0.0000	0.0000	0.0000	NA	NA	NA	NA	NA
Osteogenic	RUNX2	4.6820	3.7449	-0.9371	-1.7099	-0.1643	0.0360	0.1441	0.0263	0.0906	-1.0000
Osteogenic	ALPL	2.8568	1.3669	-1.4899	-2.9337	-0.0461	0.0935	0.1870	0.0453	0.0906	-0.8095
Osteogenic	BGLAP	0.3887	0.2468	-0.1418	-0.5837	0.3000	0.5896	0.5896	0.4468	0.5958	-0.3333

Panel	Gene	Ref mean	Treat mean	Mean diff	Ci lower	Ci upper	Wilcox p-value	Wilcox P-adj	t_p	t_padj	Rank biserial
Osteogenic	SPP1	0.2251	0.2196	-0.0055	-0.3783	0.3674	0.4017	0.5356	0.9713	0.9713	-0.4286
Chondrogenic	SOX9	3.6047	3.5847	-0.0200	-0.5067	0.4667	0.8339	0.8339	0.9201	0.9201	0.1429
Chondrogenic	COL2A1	0.0127	0.0000	-0.0127	-0.0334	0.0080	0.3711	0.7422	0.1747	0.3494	-1.0000
Chondrogenic	ACAN	0.0000	0.0000	0.0000	0.0000	0.0000	NA	NA	NA	NA	NA
Lipid ppar	SCD	7.6673	5.9768	-1.6905	-2.4719	-0.9090	0.0360	0.0360	0.0026	0.0033	-1.0000
Lipid ppar	HMGCS1	6.6244	4.9702	-1.6541	-2.0465	-1.2618	0.0360	0.0360	0.0001	0.0003	-1.0000
Lipid ppar	SORBS1	0.5210	0.1497	-0.3712	-0.5521	-0.1904	0.0360	0.0360	0.0033	0.0033	-1.0000
Hedgehog wnt	GLI1	1.9064	0.7357	-1.1707	-1.6682	-0.6732	0.0360	0.0360	0.0018	0.0028	-1.0000
Hedgehog wnt	GLI2	3.0094	1.6203	-1.3892	-1.9849	-0.7934	0.0360	0.0360	0.0019	0.0028	-1.0000
Hedgehog wnt	WNT3	1.3856	0.6636	-0.7220	-1.1472	-0.2967	0.0360	0.0360	0.0073	0.0073	-1.0000
Efferocytosis immune	PECAM1	1.1013	1.8630	0.7617	0.1559	1.3675	0.0360	0.0789	0.0231	0.0542	1.0000
Efferocytosis immune	DUSP4	2.8313	4.2219	1.3906	0.0871	2.6942	0.0592	0.0789	0.0407	0.0542	0.9048
Efferocytosis immune	DUSP10	5.0632	5.8751	0.8119	-0.2058	1.8296	0.1422	0.1422	0.0956	0.0956	0.7143
Efferocytosis immune	PTGER2	2.8942	4.9573	2.0631	0.2293	3.8969	0.0592	0.0789	0.0341	0.0542	0.9048

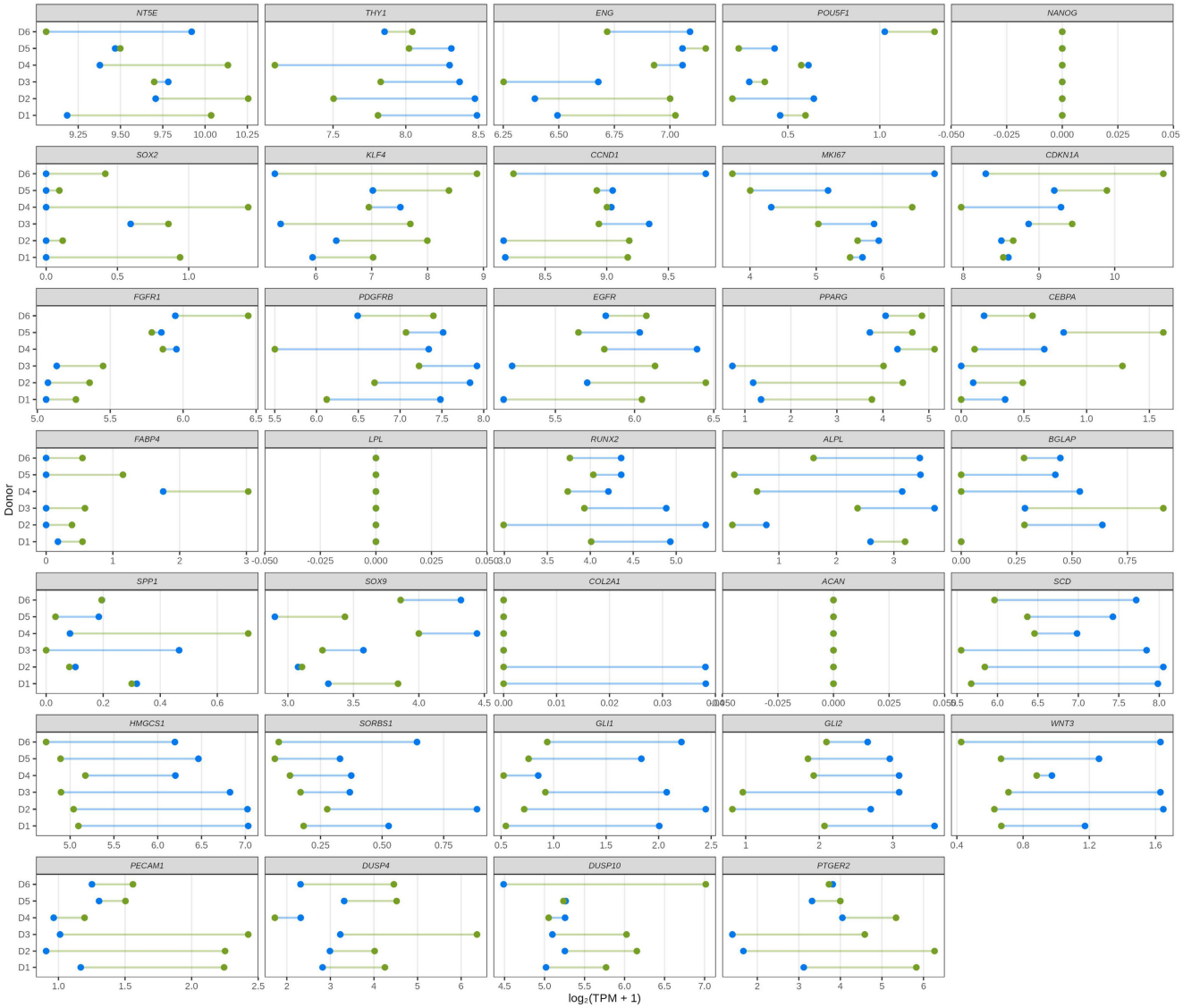


Figure 8. Donor-level transcriptomic shifts associated with autoserum-driven reprogramming across the six-donor cohort. Dumbbell plots showing paired gene expression [$\log_2$(TPM + 1)] in SMSC HPL (blue) vs. SMSC Auto (green) for six independent donors. Grey connecting segments indicate magnitude and direction of shift. Panels: (A) Immunophenotypic markers; (B) Stemness; (C) Adipogenic markers; (D) Osteogenic markers; (E) Chondrogenic markers; (F) Proliferation signatures; (G) Mitogenic receptors; (H) Hedgehog/Wnt; (I) Efferocytosis/immune; (J) Lipid/PPAR metabolism. Paired mean differences (effect sizes) and 95% confidence intervals for each gene are reported in Table 2.

The selection of adult, non-foreskin skin tissue addresses a fundamental limitation in current research, which has predominantly relied on neonatal or pediatric samples. Adult skin provides a minimally invasive procurement route that, in principle, is not restricted by donor sex, in contrast to foreskin-derived sources. Beyond accessibility, the embryological heterogeneity of the dermal niche represents a biologically plausible, though not yet experimentally demonstrated, basis for exploring skin as an MSC source [38, 39]. Unlike adipose tissue, which is exclusively mesodermal in origin, the skin dermis harbors cells derived from multiple embryonic lineages. However, the present study does not provide direct evidence of enhanced developmental plasticity or secretome diversity relative to adipose-derived cells, and we refrain from claiming tri-germ-layer superiority without functional or secretomic comparative data.

The concept of disease microenvironment preconditioning (DMP) suggests that exposing MSCs to patient-derived serum or body fluids may strengthen their adaptation to the post-infusion environment. This framework has previously been explored using inflammatory cytokine cocktails and hypoxic preconditioning; our approach differs by using an undefined, donor-specific serum product. Because donor clinical/disease status was not systematically characterized in this cohort (see Limitations), the present transcriptomic shifts should be interpreted as evidence of a response to a donor-specific blood-derived supplement rather than confirmed disease-specific preconditioning. Despite a significant reduction in human platelet lysate supplementation, the addition of autoserum was associated with accelerated proliferation and higher cumulative expansion levels. This proliferative phenotype may be associated with the nominally significant upregulation of stemness factors SOX2 ($p = 0.036$, FDR = 0.089) and KLF4 ($p = 0.059$, FDR = 0.089) observed in our cohort; PDGFRB, in contrast, exhibited a decrease in the primed group and did not reach statistical significance ($p = 0.142$, FDR = 0.213), and its contribution to the observed proliferative phenotype remains unclear and warrants further investigation. While these stemness changes did not survive multiple-testing correction, their consistent directional trends across all six donors, combined with the proliferative phenotype observed functionally, suggest biological relevance that warrants validation in larger cohorts. Cytokine/chemokine profiling of the autoserum product itself was not performed in this study; such characterization would be required to substantiate the DMP framework and is identified as a priority for future work.

We note an apparent discrepancy between the adipogenic phenotype (Oil Red O staining performed after differentiation induction) and the basal transcriptomic profile (RNA sequencing performed on undifferentiated cells at Passage 5, prior to induction). Because these two datasets reflect different cellular states and time points, the reduced expression of SCD and HMGCS1 at baseline cannot be directly interpreted as a mechanistic driver of, or paradox with, the subsequent adipogenic outcome. Resolving this relationship would require transcriptomic profiling during or after adipogenic induction, which was beyond the scope of the present study. With this caveat, the observed downregulation of key metabolic regulators (SCD, HMGCS1, SORBS1; all $p = 0.036$, FDR = 0.036) in undifferentiated primed cells may reflect a baseline metabolic state that is distinct from that of standard-condition cells, potentially involving altered lipid flux or utilization of exogenous lipids provided by the autoserum supplement [40-42]. The concurrent nominally significant upregulation of PPARG ($p = 0.036$, FDR = 0.054) and FABP4 ($p = 0.036$, FDR = 0.054), which did not survive FDR correction, further complicates straightforward interpretation. Post-transcriptional regulation, including miRNA-mediated repression or altered protein stability, may also decouple mRNA abundance from enzymatic activity, as has been reported for SCD and HMGCS1 in metabolically active tissues. We emphasize that these observations are hypothesis-generating and that a direct mechanistic link between the baseline transcriptomic signature and the functional adipogenic outcome cannot be established from the present data.

A potentially relevant observation in our transcriptomic analysis is the modulation of the efferocytosis and immune regulation network. The nominally significant upregulation of PECAM1 ($p = 0.036$, FDR = 0.079), while not surviving FDR correction, showed a consistent directional change across all six donors (rank-biserial $r = 1.0$). However, PECAM1 upregulation could reflect a discrete $CD31^+$ subpopulation (such as endothelial-like cells or vascular stromal contamination) rather than a uniform shift across the SMSC population; validating CD31 protein expression by flow cytometry is identified as a priority follow-up. The consistent upward trends in regulators such as DUSP4 ($p = 0.059$, FDR = 0.079), a known inhibitor of inflammatory MAPK signaling, are consistent with a transcriptomic shift toward inflammatory resolution [43, 44]. It should be noted that these immunomodulatory changes, while directionally consistent, did not achieve statistical significance after multiple-testing correction and should be interpreted as hypothesis-generating trends

requiring validation in larger cohorts. The downregulation of Hedgehog and Wnt pathway components (GLI1, GLI2, WNT3; all FDR = 0.036) indicates modulation of developmental signaling associated with proliferation, differentiation, and stem cell maintenance; whether this shift corresponds to a specific functional phenotype was not directly tested in this study. Whether this transcriptomic signature translates into reduced fibrotic or scarring potential *in vivo* requires functional validation, such as fibroblast co-culture or *in vivo* wound/fibrosis models, which were beyond the scope of the present study.

These transcriptomic shifts suggest a hypothesis-generating rationale for further investigating autoserum-primed skin-derived cells in immune-mediated clinical applications; this interpretation is based solely on gene expression changes and has not been functionally validated in the present study. Direct functional validation of immunomodulatory capacity, such as PBMC/T-cell suppression assays, macrophage polarization and efferocytosis co-culture, IFN-γ/TNF-α challenge with cytokine inhibition readouts, and IDO1/PGE2 secretion measurement, represents the necessary next step to substantiate the transcriptomic findings reported here. The T-cell suppression and cytokine (IL-2/IFN-γ) inhibition assay methodology has been established and validated by our group for peripheral blood-derived MSCs [45], providing a feasible pathway for follow-up validation. By exposing cells to host circulating factors before infusion, the priming strategy may precondition cells toward an immunologically alert state, though whether this translates into enhanced macrophage-mediated clearance of apoptotic cells or immune tolerance within allograft microenvironments requires confirmation through functional co-culture and *in vivo* studies.

Study Limitations and Future Directions

Several limitations should be acknowledged. First, the study cohort of six paired donors represents a modest sample. While transcriptomic shifts were directionally consistent across most of the six donor pairs, substantial inter-donor variability was observed in several differentiation datasets (Figures 3-5) and target genes (including NT5E, ENG, LPL, CCND1, and SOX9), including donors showing bidirectional responses. This variability should be considered alongside the average trends reported here, and future studies with larger and clinically characterized cohorts are required to resolve its source [46]. Second, the experimental design compares SMSC + 5% HPL against SMSC + 2% HPL + autoserum, in which HPL concentration and autoserum supplementation inclusion vary simultaneously. This precludes attributing the observed proliferative and transcriptomic changes specifically to autoserum rather than to HPL reduction; a dedicated 2% HPL-only control arm is an essential experiment for follow-up studies. Third, the present study evaluated autoserum priming only through Passage 5; whether this strategy can be sustained beyond this point while preserving MSC phenotype, viability, and multipotency was not assessed and represents an important direction for future work, particularly for applications requiring larger cell numbers. Fourth, scalability of this protocol to clinically relevant cell numbers (for example, via closed-system bioreactors or multilayer flasks) was not evaluated and remains to be established. Fifth, direct comparison with FBS-expanded cells, historically the reference standard prior to the adoption of HPL-based xeno-free systems, was not performed in this study. Sixth, ADMSCs in this study were cultured under standard 5% HPL conditions only and were not exposed to autoserum; the comparison therefore reflects SMSC + autoserum reaching a level of adipogenic output statistically indistinguishable from standard-condition ADMSC, not a direct head-to-head comparison under identical priming exposure. Seventh, sterility, mycoplasma, and endotoxin testing were not performed in this exploratory study; these release-criteria assessments are necessary prerequisites before any clinical manufacturing claim can be made. Eighth, cytokine and chemokine profiling of the autoserum product was not performed; such characterization would be required to substantiate the DMP framework. Ninth, functional validation of immunomodulatory capacity (T-cell suppression, macrophage co-culture, efferocytosis, IDO1/PGE2 secretion) was not included; the transcriptomic trends reported here require functional confirmation. Tenth, chondrogenesis was evaluated primarily by pellet diameter, a non-specific measure of matrix accumulation; quantitative endpoints such as GAG/DNA content, quantitative Alcian Blue absorbance, or COL2A1/ACAN/SOX9 expression would provide more specific confirmation. Eleventh, meeting ISCT minimal criteria (spindle morphology, CD73/CD90/CD105 positivity, hematopoietic marker negativity) does not uniquely distinguish MSCs from dermal fibroblasts, which share these features; additional characterization such as colony-forming unit-fibroblast (CFU-F) assay, a dedicated dermal fibroblast control, or transcriptomic comparison against reference stromal populations would be required to more rigorously establish MSC identity. In the absence of such data, the term "skin-derived stromal cells (SMSCs)" is used descriptively rather than as a claim of a molecularly distinct MSC

population. Finally, autologous MSC products avoid the alloimmune sensitization risk associated with allogeneic sources, but this advantage is offset by longer manufacturing timelines, donor-specific quality-control requirements, and the possibility of reduced proliferative and differentiation capacity in older or chronically ill donors. These considerations underscore the rationale for priming strategies, such as the combined reduced-HPL/autoserum approach evaluated here, aimed at compensating for donor-to-donor variability in autologous cell products.

Conclusions

This study establishes human adult skin dermis as a minimally invasive and readily accessible source of mesenchymal stromal cells that meets ISCT immunophenotypic and trilineage differentiation criteria. The results demonstrate that skin-derived cells from adult donors maintain an immunophenotype compliant with international standards and exhibit trilineage differentiation potential, with quantitative osteogenic output lower than adipose-derived counterparts but chondrogenic pellet expansion comparable between cell types. A combined reduced-HPL/autoserum priming paradigm is associated with enhanced *ex vivo* expansion and consistent transcriptomic shifts spanning metabolic remodeling and developmental pathway modulation. This strategy increased lipid vacuole formation in skin-derived cells within the study cohort, though formal equivalence with adipose-derived cells was not established.

Across the six independent donors, the priming paradigm was associated with FDR-significant downregulation of developmental pathways, including Hedgehog and Wnt signaling (GLI1, GLI2, WNT3; all FDR = 0.036), and key lipid and PPAR metabolic regulators (SCD, HMGCS1, SORBS1; all FDR = 0.036). These changes surviving multiple-testing correction represent the core transcriptomic signature of the combined priming approach. Additional nominally significant trends, including upregulation of PECAM1 (FDR = 0.079), SOX2 (FDR = 0.089), and adipogenic markers PPARG and FABP4 (FDR = 0.054), showed consistent directional changes across all donors and may reflect biologically relevant shifts that require validation in larger cohorts. Collectively, these findings identify the reduced-HPL/autoserum priming paradigm as a transcriptomically distinct culture strategy that merits further functional investigation. Upregulation of PECAM1 alone is insufficient to establish immunomodulatory readiness or personalized therapeutic responsiveness; these remain hypotheses to be tested through dedicated functional assays before this platform can be considered potentially translatable or applied to specific indications such as solid organ transplantation.

Abbreviations

Mesenchymal stromal cells: MSCs; Skin-derived MSCs: SMSCs; Adipose-derived MSCs: ADMSCs; Human platelet lysate: HPL; Population doubling time: PDT; Population doubling level: PDL; Principal component analysis: PCA; Extracellular vesicles: EVs; International Society for Cell & Gene Therapy: ISCT; Fetal bovine serum: FBS; Disease Microenvironment Preconditioning: DMP; Oil Red O: ORO; Alizarin Red S: ARS; Transcripts per million: TPM; Differentially expressed genes: DEGs.

Acknowledgments

The authors express their sincere gratitude to Dr. Chung-Chuan Hsiung and the staff at Bo-Ai Clinic (Kaohsiung, Taiwan) for their invaluable assistance and technical expertise in the isolation and purification of skin mesenchymal stromal cells (SMSCs).

Financial support and sponsorship

This work was supported by grants from the Ministry of National Defense-Medical Affairs Bureau (MND-MAB-C15-114-063, MND-MAB-C15-114-064, MND-MAB-C15-114-065, and MND-MAB-C15-114-066) and the National Science and Technology Council, Taiwan (NSTC 115-2314-B-532-009).

Ethics statement

This study was approved by the Institutional Review Board of Armed Forces Kaohsiung General Hospital (approval no. KAFGHIRB-114-001). All procedures were performed in accordance with the ethical standards of the Declaration of Helsinki, and written informed consent was obtained from all participants prior to inclusion.

Data availability statement

The raw and processed RNA-seq data supporting the findings of this study have been deposited in the NCBI Gene Expression Omnibus (GEO) under accession number GSE341711. Raw proliferation kinetics data (PDT and PDL values across passages for each donor) are available from the corresponding authors upon reasonable request. Total nucleated cell yield from initial tissue digestion, Passage 1 proliferation data, and autologous serum yield per donor were not systematically recorded and are acknowledged as a limitation. All other source data, including flow cytometry histograms and differentiation assay quantifications, are available

from the corresponding authors upon reasonable request.

Competing Interests

The authors have declared that no competing interest exists.

References

1. Squillaro T, Peluso G, Galderisi U. Clinical Trials With Mesenchymal Stem Cells: An Update. Cell Transplant. 2016; 25: 829-48.
2. Pittenger M, Discher D, Péault B, Phinney D, Hare J, Caplan A. Mesenchymal stem cell perspective: cell biology to clinical progress. npj Regen Med. 2019; 4: 22.
3. Long Q. From "stem" to "stromal": Reframing the nomenclature of mesenchymal stromal cell therapy. Cell Transplant. 2025; 34: 9636897251385288.
4. Caplan A. Mesenchymal Stem Cells: Time to Change the Name! Stem Cells Transl Med. 2017; 6: 1445-51.
5. Phinney D, Pittenger M. Concise Review: MSC-Derived Exosomes for Cell-Free Therapy. Stem Cells. 2017; 35: 851-8.
6. Zuk P, Zhu M, Ashjian P, De Ugarte D, Huang J, Mizuno H, et al. Human adipose tissue is a source of multipotent stem cells. Mol Biol Cell. 2002; 13: 4279-95.
7. Toma J, Akhavan M, Fernandes K, Barnabé-Heider F, Sadikot A, Kaplan D, et al. Isolation of multipotent adult stem cells from the dermis of mammalian skin. Nat Cell Biol. 2001; 3: 778-84.
8. Schallmoser K, Strunk D. Preparation of pooled human platelet lysate (pHPL) as an efficient supplement for animal serum-free human stem cell cultures. J Vis Exp. 2009.
9. Mojica-Henshaw M, Jacobson P, Morris J, Kelley L, Pierce J, Boyer M, et al. Serum-converted platelet lysate can substitute for fetal bovine serum in human mesenchymal stromal cell cultures. Cytotherapy. 2013; 15: 1458-68.
10. Hemeda H, Giebel B, Wagner W. Evaluation of human platelet lysate versus fetal bovine serum for culture of mesenchymal stromal cells. Cytotherapy. 2014; 16: 170-80.
11. Mante N, Undale V, Sanap A, Bhonde R, Tambe P, Bansode M, et al. Disease microenvironment preconditioning: An evolving approach to improve therapeutic efficacy of human mesenchymal stromal cells. Int Immunopharmacol. 2025; 157: 114701.
12. Noronha N, Mizukami A, Caliári-Oliveira C, Cominal J, Rocha J, Covas D, et al. Priming approaches to improve the efficacy of mesenchymal stromal cell-based therapies. Stem Cell Res Ther. 2019; 10: 131.
13. Ferreira J, Teixeira G, Santos S, Barbosa M, Almeida-Porada G, Gonçalves R. Mesenchymal Stromal Cell Secretome: Influencing Therapeutic Potential by Cellular Pre-conditioning. Front Immunol. 2018; 9: 2837.
14. Cheng A, Choi D, Lora M, Shum-Tim D, Rak J, Colmegna I. Human multipotent mesenchymal stromal cells cytokine priming promotes RAB27B-regulated secretion of small extracellular vesicles with immunomodulatory cargo. Stem Cell Res Ther. 2020; 11: 539.
15. Krampera M, Galipeau J, Shi Y, Tarte K, Sensebe L. Immunological characterization of multipotent mesenchymal stromal cells–The International Society for Cellular Therapy (ISCT) working proposal. Cytotherapy. 2013; 15: 1054-61.
16. Hackel A, Vollmer S, Bruderek K, Lang S, Brandau S. Immunological priming of mesenchymal stromal/stem cells and their extracellular vesicles augments their therapeutic benefits in experimental graft-versus-host disease via engagement of PD-1 ligands. Front Immunol. 2023; 14: 1078551.
17. Joshi J, Verma S, Upadhya R, Bhat S, Seetharam R. Inflammatory priming of mesenchymal stromal cells enhances its secretome potential through secretion of anti-inflammatory and ECM modulating factors: Insights into proteomic and functional properties. Biochem Biophys Res Commun. 2025; 778: 152391.
18. Chiang YC, Wang CY, Palekkode N, Yang SF, Chang KF, Ko CC, et al. Multi-Omics and Single-Cell Dissection of Exostosin Glycosyltransferases (EXT1/EXT2) Reveals Divergent Oncogenic Roles and Therapeutic Vulnerabilities in Gliomas. J Cancer. 2026; 17: 177-96.
19. Chiang YC, Wang CY, Kumar S, Hsieh CB, Chang KF, Ko CC, et al. Metal ion transporter SLC39A14-mediated ferroptosis and glycosylation modulate the tumor immune microenvironment: pan-cancer multi-omics exploration of therapeutic potential. Cancer Cell Int. 2025; 25: 363.
20. Kumar S, Tsai MC, Solomon DD, Ngadio JL, Xuan DTM, Ko CC, et al. Single-cell transcriptomics reveal PRRC1 as a malignant cell enriched driver of DNA repair and therapy resistance in glioblastoma. DNA Repair (Amst). 2026; 161: 103934.
21. Dominici M, Le Blanc K, Mueller I, Slaper-Cortenbach I, Marini F, Krause D, et al. Minimal criteria for defining multipotent mesenchymal stromal cells. The International Society for Cellular Therapy position statement. Cytotherapy. 2006; 8: 315-7.
22. Wu YJ, Chiao CC, Chuang PK, Hsieh CB, Ko CY, Ko CC, et al. Comprehensive analysis of bulk and single-cell RNA sequencing data reveals Schlafen-5 (SLFN5) as a novel prognosis and immunity. Int J Med Sci. 2024; 21: 2348-64.
23. Li CY, Anuraga G, Chang CP, Weng TY, Hsu HP, Ta HDK, et al. Repurposing nitric oxide donating drugs in cancer therapy through immune modulation. J Exp Clin Cancer Res. 2023; 42: 22.
24. Solomon DD, Ko CC, Chen HY, Kumar S, Wulandari FS, Xuan DTM, et al. A machine learning framework using urinary biomarkers for pancreatic ductal adenocarcinoma prediction with post hoc validation via single-cell transcriptomics. Brief Bioinform. 2025; 26.
25. Anuraga G, Wang WJ, Phan NN, An Ton NT, Ta HDK, Berenice Prayugo F, et al. Potential Prognostic Biomarkers of NIMA (Never in Mitosis, Gene A)-Related Kinase (NEK) Family Members in Breast Cancer. J Pers Med. 2021; 11.
26. Cheng LC, Kao TJ, Phan NN, Chiao CC, Yen MC, Chen CF, et al. Novel signaling pathways regulate SARS-CoV and SARS-CoV-2 infectious disease. Medicine (Baltimore). 2021; 100: e24321.
27. Choy TK, Wang CY, Phan NN, Khoa Ta HD, Anuraga G, Liu YH, et al. Identification of Dipeptidyl Peptidase (DPP) Family Genes in Clinical Breast Cancer Patients via an Integrated Bioinformatics Approach. Diagnostics (Basel). 2021; 11.
28. Chiao CC, Liu YH, Phan NN, An Ton NT, Ta HDK, Anuraga G, et al. Prognostic and Genomic Analysis of Proteasome 20S Subunit Alpha (PSMA) Family Members in Breast Cancer. Diagnostics (Basel). 2021; 11.
29. Ta HDK, Wang WJ, Phan NN, An Ton NT, Anuraga G, Ku SC, et al. Potential Therapeutic and Prognostic Values of LSM Family Genes in Breast Cancer. Cancers (Basel). 2021; 13.
30. Xuan DTM, Wu CC, Kao TJ, Ta HDK, Anuraga G, Andriani V, et al. Prognostic and immune infiltration signatures of proteasome 26S subunit, non-ATPase (PSMD) family genes in breast cancer patients. Aging (Albany NY). 2021; 13: 24882-913.
31. Palekkode N, Liu CH, Chen JB, Solomon DD, Kumar S, Ko CC, et al. Multi-omics profiling identifies ACP2 as a lysosome-associated biomarker linked to immune dynamics and clinical outcomes in glioma. Comput Biol Chem. 2026; 124: 109165.
32. Wang CY, Chao YJ, Chen YL, Wang TW, Phan NN, Hsu HP, et al. Upregulation of peroxisome proliferator-activated receptor-α and the lipid metabolism pathway promotes carcinogenesis of ampullary cancer. Int J Med Sci. 2021; 18: 256-69.
33. Liu HL, Yeh IJ, Phan NN, Wu YH, Yen MC, Hung JH, et al. Gene signatures of SARS-CoV/SARS-CoV-2-infected ferret lungs in short- and long-term models. Infect Genet Evol. 2020; 85: 104438.
34. Liu YW, Lee YK, Chang KF, Hsieh CB, Chang CH, Ko CC, et al. Integrative Analysis of Glycosylation-Related Genes Reveals Prognostic Subtypes, Immune Evasion, and Therapeutic Vulnerabilities in Lung Adenocarcinoma. Oncol Res. 2026; 34: 18.
35. Solomon DD, Lee YK, Kumar S, Chang KF, Lin CH, Ko CC, et al. Multiomics, pharmacogenomic, and structural characterization of NCCRP1 as a candidate therapeutic target in ovarian cancer. Naunyn Schmiedebergs Arch Pharmacol. 2026.
36. Solomon DD, Lin HR, Lee YK, Kumar S, Ko CC, Chang KF, et al. Multi-level Transcriptomic and Machine-learning Analyses Identify MZT1 as a Proliferation-associated Prognostic Marker in Lung Adenocarcinoma. Cancer Genomics Proteomics. 2026; 23: 996-1020.
37. Hsu WH, Chang KF, Chang CH, Lin HR, Wu CJ, Ko CC, et al. Multi-Omics and Single-Cell Dissection Reveals EXT1 as a Glycosylation-Linked Therapeutic Target in Cancer. Oncol Res. 2026; 34: 19.
38. Kuroda Y, Kitada M, Wakao S, Nishikawa K, Tanimura Y, Makinoshima H, et al. Unique multipotent cells in adult human mesenchymal cell populations. Proc Natl Acad Sci U S A. 2010; 107: 8639-43.
39. Costa L, Eiro N, Fraile M, Gonzalez L, Saá J, Garcia-Portabella P, et al. Functional heterogeneity of mesenchymal stem cells from natural niches to culture conditions: implications for further clinical uses. Cell Mol Life Sci. 2021; 78: 447-67.
40. Liu L, Liu H, Chen M, Ren S, Cheng P, Zhang H. miR-301b miR-130b—PPARγ axis underlies the adipogenic capacity of mesenchymal stem cells with different tissue origins. Sci Rep. 2017; 7: 1160.
41. Wu L, Cai X, Dong H, Jing W, Huang Y, Yang X, et al. Serum regulates adipogenesis of mesenchymal stem cells via MEK/ERK-dependent PPARgamma expression and phosphorylation. J Cell Mol Med. 2010; 14: 922-32.

42. Souza-Moreira L, Soares V, Dias S, Bozza P. Adipose-derived Mesenchymal Stromal Cells Modulate Lipid Metabolism and Lipid Droplet Biogenesis via AKT/mTOR-PPARγ Signalling in Macrophages. Sci Rep. 2019; 9: 20304.
43. Sheng Y, Hu W, Chen S, Zhu X. Efferocytosis by macrophages in physiological and pathological conditions: regulatory pathways and molecular mechanisms. Front Immunol. 2024; 15: 1275203.
44. Doran A, Yurdagul A, Tabas I. Efferocytosis in health and disease. Nat Rev Immunol. 2020; 20: 254-67.
45. Ma J, Hsiung C, Yang T, Sun H, Kuo M. Isolate Circulating Mesenchymal Stromal Cells Without Growth Factor Administration and Using Density Gradient. Stem Cells Int. 2025; 2025: 5545892.
46. Calcat-i-Cervera S, Rendra E, Scaccia E, Amadeo F, Hanson V, Wilm B, et al. Harmonised culture procedures minimise but do not eliminate mesenchymal stromal cell donor and tissue variability in a decentralised multicentre manufacturing approach. Stem Cell Research & Therapy. 2023; 14: 120.